JPPIPA 11(9) (2025)

Jurnal Penelitian Pendidikan IPA

http://jppipa.unram.ac.id/index.php/jppipa/index

Application of GNSS Interferometric Reflectometry (GNSS-IR) for Monitoring Tidal Variations in Coastal Zones

Hairul Zulkifli[1,2*], Danar Guruh Pratomo[1], Khomsin[1]

[1] Sepuluh Nopember Institute of Technology, Surabaya, Indonesia.
[2] Meteorology, Climatology and Geophysics Agency, Indonesian.

Received: June 10, 2025
Revised: August 15, 2025
Accepted: September 25, 2025
Published: September 30, 2025

Corresponding Author:
Hairul Zulkifli
hairul.zulkifli@bmkg.go.id

DOI: 10.29303/jppipa.v11i9.12539

Abstract: GNSS-Interferometric Reflectometry (GNSS-IR) utilizes Signal-to-Noise Ratio (SNR) data from GNSS satellites to estimate sea level variations. This study applied GNSS-IR using GPS L1 SNR data from four CORS stations (CBEL, CLKI, CHAI, CLMP), paired with their nearest tide gauge stations (BLTG, LBKI, AMHI, LMPA) for validation. Data in RINEX 2.11 format at 30-second intervals were processed, considering antenna heights above the sea surface to extract reflection frequencies. Results indicate strong agreement at the LMPA (r = 0.94, RMSE = 0.17 m) and BLTG (r = 0.90, RMSE = 0.37 m) pairs, demonstrating the reliability of GNSS-IR under favorable conditions. The AMHI pair showed moderate correlation (r = 0.68, RMSE = 0.45 m), while the LBKI pair exhibited no meaningful correlation (r = –0.07), likely due to severe multipath disturbance and local site limitations. These findings suggest that GNSS-IR can provide cost-efficient and accurate sea level estimates, but performance is highly site-dependent and influenced by environmental and instrumental factors. The study highlights the potential of GNSS-IR to complement conventional tide gauges in Indonesia, while emphasizing the need for careful station selection and multi-frequency analysis in future applications.

Keywords: GNSS; GNSS-IR; Harmonic analysis; Signal to noise ratio (SNR); Tides

Introduction

Indonesia still has a relatively small number of tide gauge stations, especially when compared to the vast coverage of its territorial waters, which make up over two-thirds of the country's total area (Khomsin et al., 2021). This is concerning, given that rising sea levels have been scientifically identified as one of the most pressing global hazards, including for island nations like Indonesia (Handoko et al., 2021; Hsiao et al., 2024). Monitoring tides is therefore crucial, as tides reflect periodic fluctuations in sea surface height driven by the gravitational pull of the moon and sun, as well as their relative alignment with Earth (Orihan et al., 2019; Pratomo et al., 2019). These variations significantly influence maritime operations, including navigational safety, port activities, and coastal ecosystem stability. Since more than 85% of international trade moves through sea routes, an accurate understanding of tidal behavior is essential for maintaining efficient and safe transport networks (Khomsin et al., 2024). As such, obtaining accurate sea level data is critical. However, traditional tide measurement systems face challenges such as limited spatial reach, vulnerability to environmental conditions, and susceptibility to land motion and instrument errors (Yalçin, 2023).

One emerging alternative is the use of the Global Navigation Satellite System (GNSS), which encompasses all satellite-based positioning systems, whether currently in use or still under development (Khomsin et al., 2019). Among the innovations derived from GNSS technology is GNSS-Interferometric Reflectometry

How to Cite:
Zulkifli, H., Pratomo, D. G., & Khomsin. (2025). Application of GNSS Interferometric Reflectometry (GNSS-IR) for Monitoring Tidal Variations in Coastal Zones. *Jurnal Penelitian Pendidikan IPA*, *11*(9), 258–267. https://doi.org/10.29303/jppipa.v11i9.12539

(GNSS-IR), which has been increasingly adopted for monitoring the ocean surface in a cost-effective and precise manner (Li et al., 2021). GNSS-IR functions by analyzing GNSS signals reflected from the water surface. By examining the interference patterns between the direct and reflected signals, it is possible to determine the vertical distance from the antenna to the sea surface (F. Wang et al., 2024). Numerous studies have confirmed that GNSS-IR data aligns closely with results from conventional tide measurements, often reaching centimeter-level precision using relatively low-cost tools (Cahyadi et al., 2023; Williams et al., 2020; Yang et al., 2024).

Theoretically, when a GNSS antenna is positioned in an open setting adjacent to calm, expansive water—such as the example shown in Figure 1—multipath effects occur. This happens when the antenna captures not only the direct satellite signal but also the reflected one from nearby surfaces like the sea (Georgiadou et al., 1988; Larson et al., 2023). These reflected signals interfere with the direct signal, causing multipath effects in measurements such as pseudorange, carrier phase, and signal-to-noise ratio (SNR) (Axelrad et al., 2005). While multipath errors in pseudorange can be as large as 100 meters, those affecting carrier phase are usually within a few centimeters (Hofmann-Wellenhof et al., 2007). Interestingly, GNSS-IR takes advantage of this multipath phenomenon, transforming what is typically considered signal noise into a valuable source of data for monitoring sea level changes through the analysis of signal interference patterns.

The frequency of multipath interference can be determined using the equation proposed by Georgiadou et al. (1988):

$$f = \frac{2H}{\lambda} sin(e) \frac{d}{dt} \quad (1)$$

where e is the satellite elevation angle (°), H is the antenna height above the sea surface, and λ is the wavelength of the GNSS signal.

Equation (1) indicates that the frequency of the reflected signal is influenced by the antenna height, the signal wavelength, and the satellite's elevation angle. At lower elevation angles, the signal reflection path becomes longer, which in turn increases the intensity of multipath interference. This characteristic forms the basis for utilizing GNSS-IR to estimate periodic changes in sea surface height.

This study aims to utilize reflected GNSS signals to measure sea level fluctuations and to compare the results with conventional tide gauge data, thereby evaluating the strengths and limitations of the GNSS-IR method.

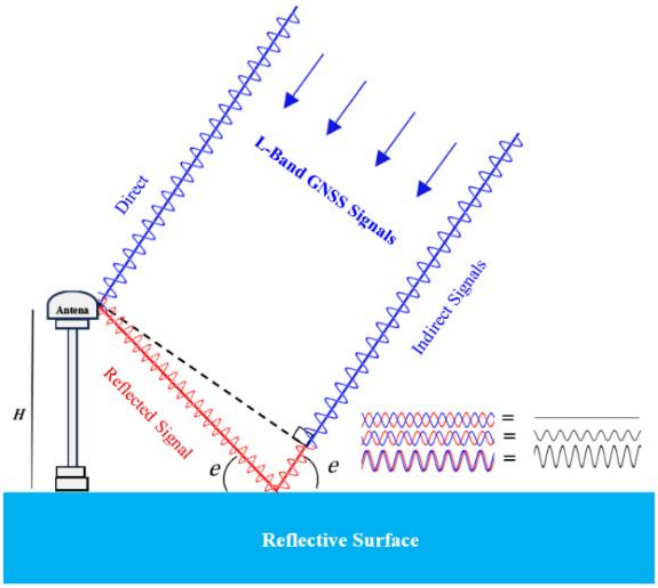

Figure 1. The direct GNSS signal (blue) and its reflected counterpart (red) interact and form a distinct interference pattern, which can be observed in the GNSS Signal-to-Noise Ratio (SNR) data. This interference pattern arises as the satellite moves along its orbital path. The frequency of this pattern depends on the vertical distance between the GNSS antenna and the reflecting surface, referred to as the reflection height (H) (Larson et al., 2023)

Method

Research Approach and Design

This study adopts a quantitative approach using a comparative study method (Bolbakov et al., 2020) to evaluate the effectiveness of the GNSS-IR technique in estimating sea surface height variations caused by tides. The primary objective of this approach is to compare sea level estimates derived from GNSS-IR with those obtained through conventional tide gauge observations. GNSS-IR works by utilizing the multipath phenomenon, where GNSS signals are reflected off the sea surface and received by a GNSS antenna located on land. By processing these reflected signals, it is possible to extract information regarding the temporal variation of sea level (Larson et al., 2013).

The GNSS-IR technique has been successfully applied across a variety of domains, including river stage monitoring (Chen et al., 2024), tsunami detection (Chai et al., 2025; Kim et al., 2021), soil moisture estimation (Chamoli et al., 2024; Padrón et al., 2025; Shekhar et al., 2024), snow depth observation (Ma et al., 2023; Yuan et al., 2024), and sea level monitoring (Ghiasi al., 2021; Peng et al., 2024; Zhu et al., 2024).

Despite these advancements, GNSS-IR still faces several technical challenges, such as estimation biases caused by tropospheric delays and inaccuracies in certain tidal components (X. Wang et al., 2022). To address these limitations, various correction methods

have been developed, including the use of the Lomb-Scargle Periodogram (LSP) and Local Mean Decomposition (LMD) techniques, both of which help enhance the long-term accuracy of GNSS-IR estimates (Wei et al., 2023, 2024).

Research Locations

This research was conducted at four coastal dockside locations across Indonesia, as illustrated in Figure 2. The selection of sites was based on the proximity between Continuously Operating Reference Stations (CORS) and nearby conventional tide gauge stations (Table 1), while also considering the diversity of coastal environmental conditions. Several factors were taken into account in choosing the study sites, including port activity levels, local topographic characteristics, and the potential for multipath interference that could affect the quality of the GNSS signals.

Table 1. List of CORS and Tide Gauge Stations Used in the Study (Source: https://srgi.big.go.id/)

CORS Station Code	Tide Gauge Station Code	Latitude	Longitude	Ellipsoidal Height (h) [m]	Location
CBEL	BLTG	-2.74	107.63	30.52	Belitung, Bangka Belitung
CLKI	LBKI	0.85	123.94	75.29	Bolaang Mongdow, North Sulawesi
CHAI	AMHI	-3.34	128.92	66.95	Central Maluku, Maluku
CLMP	LMPA	-2.78	121.04	26.25	East Luwu, South Sulawesi

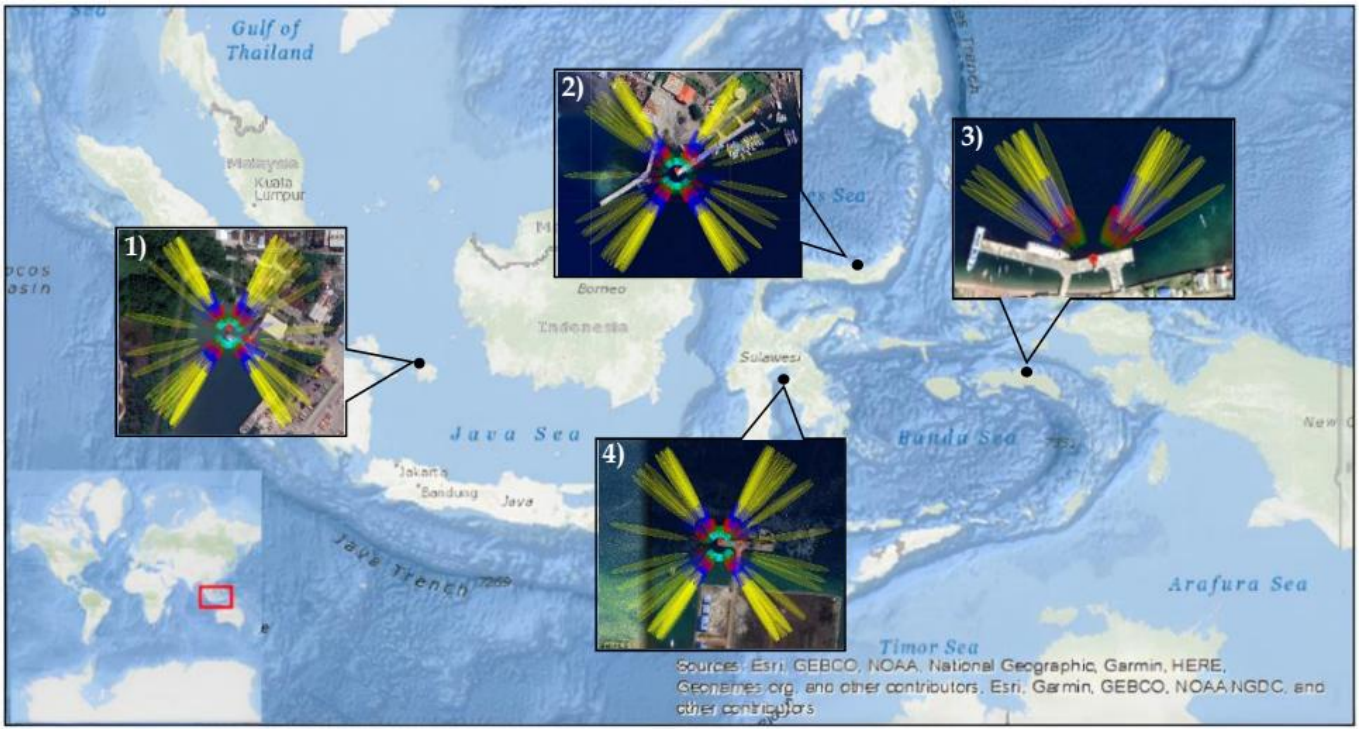

Figure 2. Research location

Data

This study utilized two primary types of data, both obtained from the Geospatial Information Agency (BIG) via the official website (https://srgi.big.go.id): (1) conventional tidal observation data and (2) GNSS observation data from Continuously Operating Reference Stations (CORS). These datasets cover the period from January to December 2024, allowing for a full annual cycle of sea level dynamics to be analyzed.

The GNSS data were recorded in RINEX 2.11 format (Pestana, 2016) with a 30-second observation interval, while the conventional tide data were collected via tide gauges at 1-minute intervals. The 12-month observation period was chosen to ensure the analysis captured daily, monthly, and seasonal tidal variations (Rajabi et al., 2022). Furthermore, this duration allows for harmonic analysis of major tidal constituents such as O_1, K_1, M_2, and S_2 (H. Wang et al., 2023), providing a comprehensive understanding of tidal characteristics at each study site.

Table 2. Summary of Data Types Used (Source: https://srgi.big.go.id)

Data type	Format	Interval
GNSS	RINEX 2.11	30 seconds
Tide gauge	*.txt	1 minute

Research Workflow

The research was structured into three primary phases: data preparation, data processing, and data analysis (Figure 3).

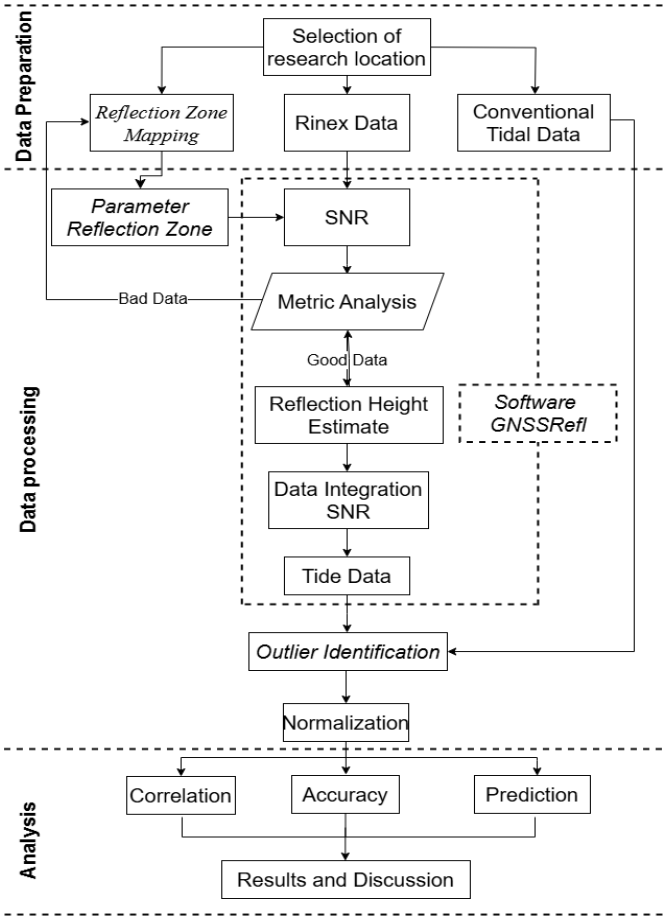

Figure 3. Research flowchart

In the data preparation phase, selection of study sites was based on the availability of continuous GNSS and tidal gauge data, proximity between CORS and tidal stations, and environmental conditions that favor effective GNSS signal reflection. GNSS observation data in RINEX 2.11 format and conventional tidal gauge records were obtained from the official platform of the Geospatial Information Agency of Indonesia (https://srgi.big.go.id). Reflection zones surrounding the GNSS antennas were delineated using the GNSS-reflections.org interface to ensure optimal multipath signal capture.

The data processing phase involved extracting signal-to-noise ratio (SNR) values from RINEX files using the Gnssrefl software (Larson, 2024). A sinusoidal model was applied to characterize the oscillatory patterns resulting from reflected signals, following the mathematical approach proposed by Roesler et al. (2018).

$$SNR(e) = A(e)\sin\left(\frac{4\pi H_R}{\lambda}\sin e + \emptyset\right) \quad (2)$$

Outliers were eliminated using the Interquartile Range (IQR) method (Mahmoodi et al., 2018), and data normalization was conducted through Min-Max Scaling to standardize both GNSS-IR and tidal datasets for comparative analysis (Ha et al., 2012).

The data analysis phase comprised several statistical assessments to evaluate the effectiveness of the GNSS-IR technique. Pearson correlation was applied to determine the strength of the linear relationship between GNSS-IR-derived and tide gauge-observed sea surface heights. Additionally, Root Mean Square Error (RMSE) and Mean Absolute Error (MAE) were calculated to assess the accuracy and consistency of the estimations.

Further, tidal harmonic analysis was conducted using the *T_Tide* toolbox in MATLAB to extract dominant tidal constituents (O_1, K_1, M_2, and S_2) from both GNSS-IR and conventional tide data. The Formzahl number was computed to classify the prevailing tidal types at each location based on the relative amplitudes of the diurnal and semidiurnal components.

Result and Discussion

Sea Surface Characterization Based on GNSS Signal Reflections

The GNSS-IR signal extraction process was conducted using L1 GPS signals at a frequency of 1575.42 MHz from four selected CORS stations: CBEL, CLKI, CHAI, and CLMP (Lombardi et al., 2001). The processed data produced key parameters such as variations in Reflector Height (RH), azimuth direction of reflections, signal amplitude, and peak-to-noise ratio/P2N (Figure 4).

The analysis revealed that each station exhibited distinct RH patterns, as summarized in Table 3. Among the stations, CLMP recorded the highest amplitude and P2N values, indicating the presence of strong and consistent multipath reflections from the surrounding sea surface (Soulat et al., 2004). Conversely, CBEL displayed stable RH estimates, demonstrating that L1 GPS signals can yield reliable sea level estimations under favorable conditions (Lei et al., 2023).

Table 3. GPS L1 Signal Extraction Results

CORS Station	Range RH (m)	Reflection Azimuth (°)	Amplitude (V/V)	P2N
CBEL	4 – 10	210 – 230	10 – 35	3 – 7
CLKI	0 – 15	10 – 35	5 – 35	2 – 8
CHAI	4 – 8	305 – 330	5 – 12.5	2 – 8
CLMP	7 – 11	195 – 225	20 – 35	5 – 9

Unlike CBEL and CLMP, the CHAI station exhibited a narrower RH range and lower signal amplitude, suggesting weaker multipath reflections at that site. In contrast, CLKI showed accurate sea level estimations. Previous studies have emphasized that both signal amplitude and noise ratio significantly influence the quality of RH estimation in GNSS-IR applications (Ding et al., 2023; Wei et al., 2024).

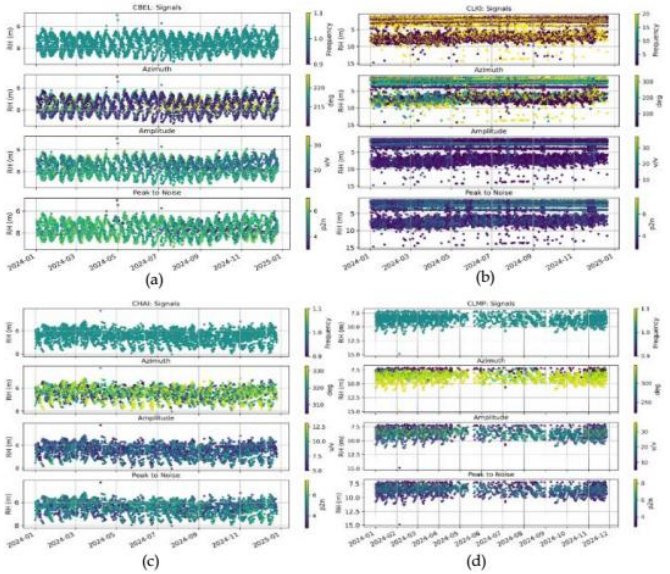

Figure 4. GNSS-IR signals extracted from GPS L1, (a) CBEL station, (b) CLKI station, (c) CHAI station, (d) CLMP station

Accuracy of GNSS-IR Tide Estimation

The analysis of GNSS-IR data from BLTG and AMHI tide gauge stations indicates that the observed sea surface fluctuations closely follow the patterns recorded by conventional tide gauges, as illustrated in Figures 5.a and 5.c. The correlation coefficients for BLTG and AMHI are 0.90 and 0.68, respectively (Table 4). The scatter plots in Figures 5.a and 5.c show a clear positive linear trend, suggesting a good agreement between GNSS-IR derived sea levels and conventional tide gauge observations. These results confirm thatGNSS-IR is capable of reliably capturing tidal variations, particularly in locations with stable multipath conditions and consistent reflective surface characteristics.

In contrast, the results from the LBKI station reveal a significant discrepancy between GNSS-IR and tide gauge data (Figure 6.b). The correlation coefficient is negative (-0.07), accompanied by relatively high RMSE and MAE values of 0.92 m and 0.74 m, respectively (Table 4). The scatter plot in Figure 6.b displays a random distribution with no clear linear pattern, indicating low reliability of GNSS-IR estimations at this site.

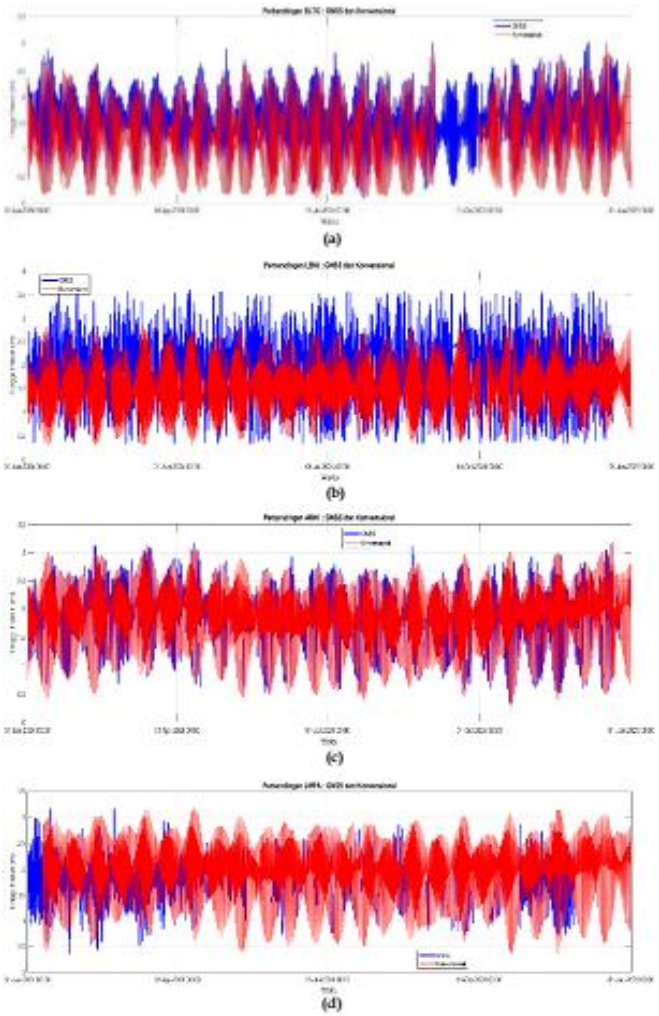

Figure 5. Comparison of GNSS-IR tidal graphs and conventional data for the period 2024, (a) BLTG station, (b) LBKI station, (c) AMHI station, (d) LMPA station

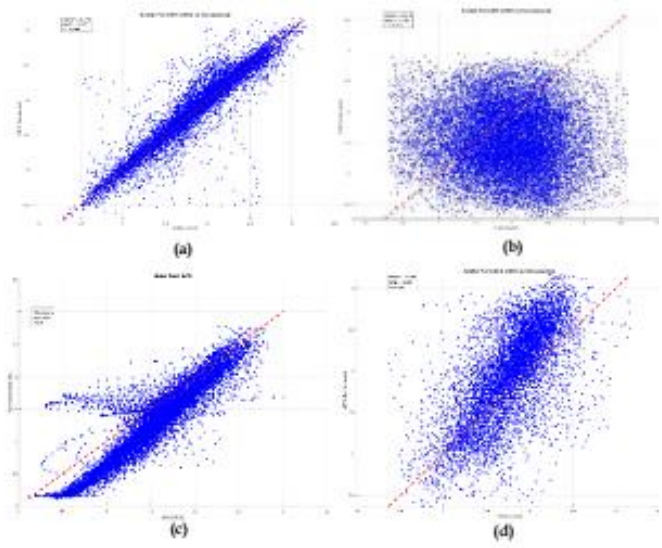

Figure 6. Scatter plot of GNSS-IR tidal and conventional data in the period 2024, (a) BLTG station, (b) LBKI station, (c) AMHI station, (d) LMPA station

On the other hand, the highest accuracy was achieved at the LMPA station, with a correlation coefficient of 0.94, and the lowest RMSE and MAE values of 0.18 m and 0.11 m, respectively. The variation in accuracy across stations is likely attributed to differences in local multipath environments and reflective surface conditions surrounding each GNSS antenna. As demonstrated by Roussel et al. (2015), unstable reflective environments can degrade the quality of multipath reflections, directly impacting the accuracy of GNSS-IR sea level estimations.

Table 4. RMSE Values and Correlation Coefficients of GNSS-IR Observations on GPS L1 Signals

Tide Station	RMSE (m)	MAE (m)	Correlation Coefficient
BLTG	0.37	0.31	0.90
LBKI	0.92	0.74	-0.07
AMHI	0.45	0.36	0.68
LMPA	0.18	0.11	0.94

Tidal Prediction

Harmonic analysis is a commonly used approach to model tidal fluctuations by utilizing the summation of the various harmonic components that comprise them (Pan et al., 2023). In this study, tidal harmonic constants were calculated at four observation locations: BLTG, LBKI, AMHI, and LMPA using MATLAB software. The analysis focused primarily on the four dominant tidal components: O_1, K_1, M_2, and S_2 (Table 5).

Based on the data in Table 5, it can be seen that the level of agreement between the GNSS-IR and conventional methods varies depending on the location. At the BLTG Station, the results from both methods tend to be similar, with the largest amplitude difference of 0.09 m in the K1 component and adjacent Formzahl Number (FN) values (15.57 for the conventional method and 20.84 for the GNSS-IR), indicating diurnal tidal characteristics. Conversely, at LBKI, significant differences occur, particularly in the semidiurnal component, where the amplitude of the GNSS-IR method is much smaller, causing a change in the tidal

type from mixed semidiurnal (FN 0.34) to diurnal (FN 3.68). Meanwhile, at AMHI, the two methods produce nearly identical values in terms of amplitude, phase, and FN (0.88), indicating that GNSS-IR is quite accurate in depicting the balanced mixed tidal type at that location. For LMPA, although differences in amplitude were found in several components, the FN values between the two methods were still close (0.68 and 0.70), so that the tidal type classification remained unchanged, namely mixed semidiurnal.

Based on the data presented in Table 5, the degree of agreement between the GNSS-IR and conventional methods varies depending on the observation site. At the BLTG station, the results from both approaches are relatively consistent, with the largest amplitude discrepancy being only 0.09 m for the K1 tidal component. The Formzahl Number (FN) values are also comparable—15.57 for the conventional method and 20.84 for GNSS-IR—indicating a diurnal tidal characteristic.

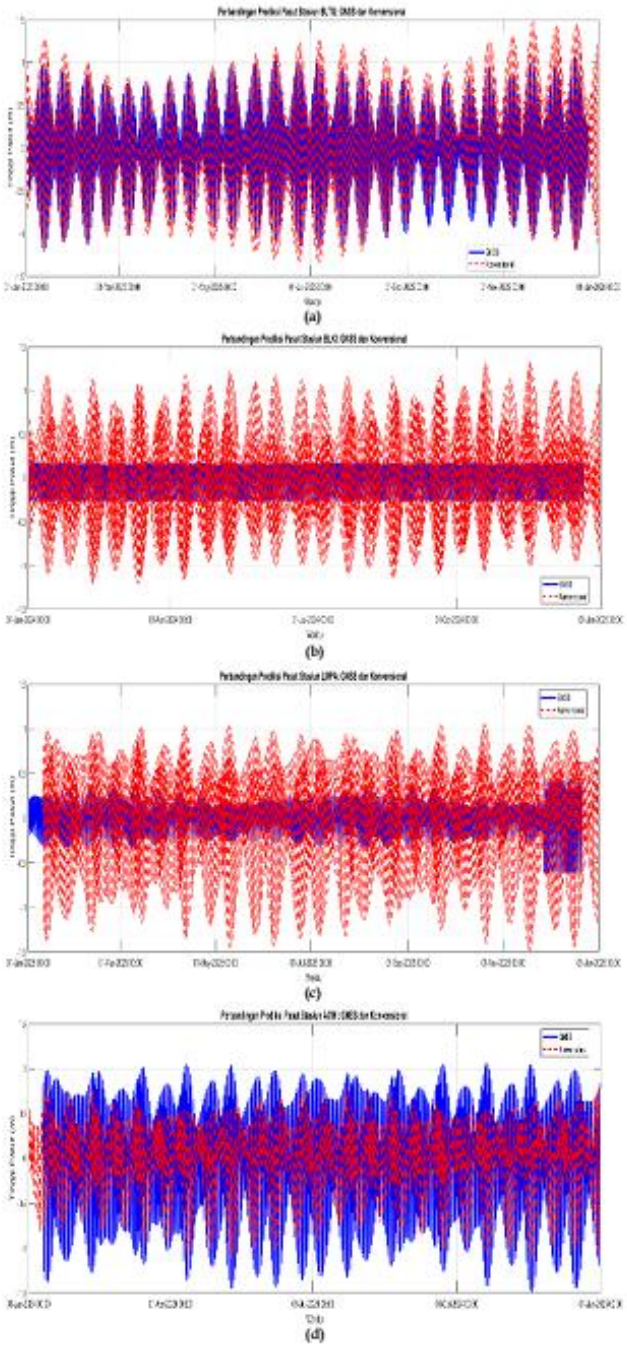

Figure 7. Comparison of tidal prediction graphs between GNSS-IR and conventional methods for the year 2025: (a) BLTG station, (b) LBKI station, (c) AMHI station, and (d) LMPA station

Table 5. Comparison of Tidal Harmonic Constants from the GNSS-IR Method with Conventional Methods

Tide Station	Method	Tidal Constituent				Formzahl
		O_1 (Amp/Fase)	K_1 (Amp/Fase)	M_2 (Amp/Fase)	S_2 (Amp/Fase)	Number (FN)
BLTG	Konv	0.36 m/354.01º	0.56 m/45.17º	0.03 m/299.71º	0.03 m/170.78º	15.57
	GNSS_IR	0.33 m/345.01º	0.47 m/35.41º	0.01 m/164.95º	0.08 m/120.48º	20.84
LBKI	Konv	0.11 m/106.1º	0.20 m/127.81º	0.57 m/289.8º	0.32 m/327.76º	0.34
	GNSS_IR	0.01 m/125.25º	0.11 m/241.99º	0.017 m/346.02º	0.01 m/234.25º	3.68
AMHI	Konv	0.19 m/193.56º	0.20 m/180.09º	0.33 m/134.04º	0.11 m/198.51º	0.88
	GNSS_IR	0.19 m/193.56º	0.20 m/180.09º	0.33 m/134.04º	0.11 m/198.51º	0.88
LMPA	Konv	0.20 m/170.89º	0.31 m/184.99º	0.58 m/136.82º	0.18 m/194.93º	0.68
	GNSS_IR	0.07 m/173.49º	0.07 m/193.73º	0.15 m/130.34º	0.04 m/170.82º	0.7

In contrast, the LBKI station exhibits significant discrepancies, particularly in the semidiurnal components. The GNSS-IR method yields much lower amplitudes, which leads to a shift in the tidal classification from mixed semidiurnal (FN = 0.34) to diurnal (FN = 3.68). At AMHI, both methods produce nearly identical results in terms of amplitude, phase, and FN (0.88), suggesting that GNSS-IR can accurately represent the mixed, mainly semidiurnal tidal type at this location. Meanwhile, at LMPA, despite minor differences in the amplitudes of certain tidal constituents, the FN values remain close (0.68 and 0.70), thereby maintaining the same tidal classification as mixed semidiurnal.

This study also includes tidal prediction modeling using GNSS-IR data from 2024 as the basis for forecasting tidal conditions in 2025. The validation process was carried out by comparing GNSS-IR-based predictions with those generated by the conventional method (Figure 7). The graphical comparison reveals that the tidal variation patterns from both methods are generally similar, particularly at the BLTG and AMHI stations. The Root Mean Square Error (RMSE) of the residuals at these locations is 0.19 m and 0.25 m, respectively, indicating that the GNSS-IR method demonstrates a satisfactory level of reliability for tidal prediction.

However, at the LBKI and LMPA stations, the highest residuals were observed during daily high and low tide peaks. This discrepancy is mainly attributed to differences in the amplitude of dominant tidal constituents, particularly the M_2 component, which showed deviations of 0.56 m and 0.43 m, respectively. These inconsistencies contribute to higher overall residual values at both sites, ultimately reducing the predictive accuracy of the GNSS-IR method in those locations.

Conclusion

This study demonstrates that the GNSS–Interferometric Reflectometry (GNSS–IR) technique is reasonably effective in estimating sea surface height in coastal areas. The tide level estimates obtained through GNSS–IR exhibit strong correlations with conventional tide gauge data, along with relatively low correction values. However, since most GNSS stations are situated within harbor environments, signal interference caused by surrounding infrastructure and port activities slightly affected data quality. Despite these challenges, GNSS–IR still shows considerable potential as a promising alternative for sea level monitoring in Indonesia.

Acknowledgments

The first author would like to express his sincere gratitude to the Meteorology, Climatology, and Geophysics Agency (BMKG) for its institutional support during this research. Special thanks are extended to Danar Guruh Pratomo and Khomsin from the Sepuluh Nopember Institute of Technology (ITS), Surabaya, for their valuable input, academic guidance, and technical assistance during the preparation of this manuscript.

Author Contributions

Conceptualization, Hairul Zulkifli and Danar Guruh Pratomo; methodology, Hairul Zulkifli; software, Hairul Zulkifli; validation, Hairul Zulkifli, Danar Guruh Pratomo, and Khomsin; formal analysis, Hairul Zulkifli; investigation, Hairul Zulkifli; resources, Hairul Zulkifli; data curation, Hairul Zulkifli; writing—original draft preparation, Hairul Zulkifli; writing—review and editing, Danar Guruh Pratomo and Khomsin; visualization, Hairul Zulkifli; supervision, Danar Guruh Pratomo and Khomsin; project administration, Hairul Zulkifli; funding acquisition, Hairul Zulkifli. All authors have read and agreed to the published version of the manuscript.

Funding

This research was financially supported by the Center for Human Resource Development of the Meteorology, Climatology, and Geophysics Agency of Indonesia (PPSDM BMKG) through its internal research funding scheme. The publication cost, including the Article Processing Charge (APC), was also fully covered by PPSDM BMKG.

Conflicts of Interest

The authors declare that there are no conflicts of interest related to this study. Any potential personal or financial circumstances that could be perceived as influencing the research findings have been transparently disclosed. The

funding agency had no involvement in the design of the study, data collection, analysis, interpretation, manuscript preparation, or the decision to publish the results.

References

Axelrad, P., Larson, K., & Jones, B. (2005). Use of the correct satellite repeat period to characterize and reduce site-specific multipath errors. *Proceedings of the 18th International Technical Meeting of the Satellite Division of The Institute of Navigation, ION GNSS 2005*, *2005*(January 2005), 2638–2648. https://epic.awi.de/id/eprint/35979/

Bolbakov, R. G., Sinitsyn, A. V., & Tsvetkov, V. Y. (2020). Methods of comparative analysis. *Journal of Physics: Conference Series*, *1679*(5). https://doi.org/10.1088/1742-6596/1679/5/052047

Cahyadi, M. N., Bawasir, A., Susilo, & Arief, S. (2023). Analysis of Water Level Monitoring using GNSS Interferometric Reflectometry in River Waters. *IOP Conference Series: Earth and Environmental Science*, *1276*(1), 0–12. https://doi.org/10.1088/1755-1315/1276/1/012020

Chai, H., Chen, K., & Lin, J. (2025). Transforming Coastal GNSS Stations Into Tsunami Gauges With Adaptive Window Interferometric Reflectometry. *IEEE Transactions on Geoscience and Remote Sensing*, *63*, 1–10. https://doi.org/10.1109/TGRS.2025.3550744

Chamoli, V., Prakash, R., & Vidyarthi, A. (2024). First Pioneering Soil Moisture Estimation Software Leveraging Navigation Signals from India's NavIC Satellite. *2024 IEEE Space, Aerospace and Defence Conference (SPACE)*, 808–811. https://doi.org/10.1109/SPACE63117.2024.10667839

Chen, Z., & Jin, S. (2024). High-frequency Water Level Estimation in the Yangtze River from GNSS-Interferometric Reflectometry. *2024 Photonics & Electromagnetics Research Symposium (PIERS)*, 1–5. https://doi.org/10.1109/PIERS62282.2024.10618080

Ding, Q., Liang, Y., Liang, X., Ren, C., Yan, H., Liu, Y., Zhang, Y., Lu, X., Lai, J., & Hu, X. (2023). Soil Moisture Retrieval Using GNSS-IR Based on Empirical Modal Decomposition and Cross-Correlation Satellite Selection. *Remote Sensing*, *15*(13). https://doi.org/10.3390/rs15133218

Georgiadou, Y., & Kleusberg, A. (1988). On carrier signal multipath effects in relative GPS positioning. *Map Collector*, *13*(3), 172–179. https://doi.org/10.1007/BF03655245

Ghiasi, Y., Farzaneh, S., Parvazi, K., & Duguay, C. R. (2021). Amplitue Estimation of Dominant Tidal Constituents Using Gnss Interferometric Reflectometry Technique. *2021 IEEE International Geoscience and Remote Sensing Symposium IGARSS*, 8546–8549. https://doi.org/10.1109/IGARSS47720.2021.9554876

Ha, J., Kambe, M., & Pe, J. (2012). Data Mining. In *Data Mining: Concepts and Techniques*. Elsevier. https://doi.org/10.1016/C2009-0-61819-5

Handoko, E. Y., Richasari, D. S., & Pratomo, D. G. (2021). Seasonal and Interannual of Sea Level Variability in the Indonesian Seas using Satellite Altimetry. *IOP Conference Series: Earth and Environmental Science*, *731*(1). https://doi.org/10.1088/1755-1315/731/1/012004

Hofmann-Wellenhof, B., Lichtenegger, H., & Wasle, E. (2007). *GNSS – Global Navigation Satellite Systems GPS, GLONASS, Galileo, and more*. Vienna: Springer Vienna.

Hsiao, S. C., Fu, H. S., Wu, H. L., Liang, T. Y., Chang, C. H., Chen, Y. M., Lin, L. Y., & Chen, W. B. (2024). Impact assessment of sea level rise-induced high tide flooding and socioeconomic losses in a highly vulnerable coastal region. *Journal of Hydrology: Regional Studies*, *55*(August), 101921. https://doi.org/10.1016/j.ejrh.2024.101921

Khomsin, Mutiara Anjasmara, I., Guruh Pratomo, D., & Ristanto, W. (2019). Accuracy Analysis of GNSS (GPS, GLONASS and BEIDOU) Obsevation for Positioning. *E3S Web of Conferences*, *94*, 0–6. https://doi.org/10.1051/e3sconf/20199401019

Khomsin, Pratomo, D. G., & Rohmawati, C. N. (2021). Analysis of accuracy comparison tidal global (FES2014, TPXO9) and regional (BIG Prediction) models to the existing tides in Surabaya and surrounding waters. *IOP Conference Series: Earth and Environmental Science*, *936*(1). https://doi.org/10.1088/1755-1315/936/1/012028

Khomsin, Pratomo, D. G., Syariz, M. A., Hariyanto, I. H., & Harisa, H. C. (2024). Dense Neural Network for Classification of Seafloor Sediment using Backscatter Mosaic Feature. *BIO Web of Conferences*, *89*. https://doi.org/10.1051/bioconf/20248907004

Kim, S.-K., Park, J., Wengrove, M. E., & Dickey, J. E. (2021). Feasibility Study of GNSS Interferometric Reflectometry (GNSS-IR) For Retrieving Significant Wave Height. *2021 IEEE Specialist Meeting on Reflectometry Using GNSS and Other Signals of Opportunity (GNSS+R)*, 69–72. https://doi.org/10.1109/GNSSR53802.2021.9617691

Larson, K. M. (2024). Gnssrefl: an open source software package in python for GNSS interferometric reflectometry applications. *GPS Solutions*, *28*(4), 1–

7. https://doi.org/10.1007/s10291-024-01694-8

Larson, K. M., Löfgren, J. S., & Haas, R. (2013). Coastal sea level measurements using a single geodetic GPS receiver. *Advances in Space Research*, *51*(8), 1301–1310. https://doi.org/10.1016/j.asr.2012.04.017

Larson, K. M., & Williams, S. D. P. (2023). Water level measurements using reflected GNSS signals. *The International Hydrographic Review*, *29*(2), 66–76. https://doi.org/10.58440/ihr-29-2-a30

Lei, J., Li, W., & Zhang, S. (2023). Improving Consistency of GNSS-IR Reflector Height Estimates between Different Frequencies Using Multichannel Singular Spectrum Analysis. *Remote Sensing*, *15*(7). https://doi.org/10.3390/rs15071779

Li, Y., Yu, K., Jin, T., Chang, X., Wang, Q., & Li, J. (2021). Development of a GNSS-IR instrument based on low-cost positioning chips and its performance evaluation for estimating the reflector height. *GPS Solutions*, *25*(4), 127. https://doi.org/10.1007/s10291-021-01163-6

Lombardi, M. A., Nelson, L. M., Novick, A. N., & Zhang, V. S. (2001). Time and Frequency Measurements Using the Global Positioning System. *The International Journal of Metrology*, *8*(3), 26–33. Retrieved from http://tf.nist.gov/general/pdf/1424.pdf

Ma, P., Huang, C., Hou, J., Zhang, Y., Han, W., & Dou, P. (2023). Snow Depth Retrieval With Multiazimuth and Multisatellite Data Fusion of GNSS-IR Considering the Influence of Surface Fluctuation. *IEEE Transactions on Geoscience and Remote Sensing*, *61*, 1–14. https://doi.org/10.1109/TGRS.2023.3323642

Mahmoodi, K., & Ghassemi, H. (2018). Outlier detection in ocean wave measurements by using unsupervised data mining methods. *Polish Maritime Research*, *25*(1), 44–50. https://doi.org/10.2478/pomr-2018-0005

Orihan, M., Borisov, M., Marinković, G., & Petrović, M. V. (2019). the Influence of Ocean Tides To Determine the Earth'S Orientation Parameters. *Archives for Technical Sciences*, *2*(21), 43–53. https://doi.org/10.7251/afts.2019.1121.043o

Padrón, N., & Vorobyov, S. (2025). A GNSS-IR Aided Multispectral Satellite Data Fusion for Meter-Level Wide-Area Volumetric Soil Moisture Estimation. *ICASSP 2025 - 2025 IEEE International Conference on Acoustics, Speech and Signal Processing (ICASSP)*, 1–5. https://doi.org/10.1109/ICASSP49660.2025.10890009

Pan, H., Xu, T., & Wei, Z. (2023). A modified tidal harmonic analysis model for short-term water level observations. *Ocean Modelling*, *186*, 102251. https://doi.org/10.1016/j.ocemod.2023.102251

Peng, D., Lin, Y. N., Lee, J.-C., Su, H.-H., & Hill, E. M. (2024). Multi-constellation GNSS interferometric reflectometry for tidal analysis: mitigations for K1 and K2 biases due to GPS geometrical errors. *Journal of Geodesy*, *98*(1), 5. https://doi.org/10.1007/s00190-023-01812-3

Pestana, A. (2016). Technical Report : Reading RINEX 2 . 11 Observation Data Files António Pestana. *Observation Data Files*. https://doi.org/10.13140/RG.2.1.4888.4087

Pratomo, D. G., Khomsin, K., & Syaputra, K. (2019). Comparison of Sea Surface Variation Derived from Global Navigation Satellite System (GNSS) and Co-Tidal in Java Sea. *E3S Web of Conferences*, *94*, 8–13. https://doi.org/10.1051/e3sconf/20199401007

Rajabi, M., Hoseini, M., Nahavandchi, H., Semmling, M., Ramatschi, M., Goli, M., Haas, R., & Wickert, J. (2022). Polarimetric GNSS-R Sea Level Monitoring Using I/Q Interference Patterns at Different Antenna Configurations and Carrier Frequencies. *IEEE Transactions on Geoscience and Remote Sensing*, *60*(May). https://doi.org/10.1109/TGRS.2021.3123146

Roesler, C., & Larson, K. M. (2018). Software tools for GNSS interferometric reflectometry (GNSS-IR). *GPS Solutions*, *22*(3), 80. https://doi.org/10.1007/s10291-018-0744-8

Roussel, N., Ramillien, G., Frappart, F., Darrozes, J., Gay, A., Biancale, R., Striebig, N., Hanquiez, V., Bertin, X., & Allain, D. (2015). Sea level monitoring and sea state estimate using a single geodetic receiver. *Remote Sensing of Environment*, *171*, 261–277. https://doi.org/10.1016/j.rse.2015.10.011

Shekhar, S., Prakash, R., Pandey, D. K., & Vidyarthi, A. (2024). Vegetation-Specific Correction for Improved Soil Moisture Estimation Through Multipath Phase Analysis Using NavIC-IR. *IGARSS 2024 - 2024 IEEE International Geoscience and Remote Sensing Symposium*, 3089–3092. https://doi.org/10.1109/IGARSS53475.2024.10642110

Soulat, F., Caparrini, M., Germain, O., Lopez-Dekker, P., Taani, M., & Ruffini, G. (2004). Sea state monitoring using coastal GNSS-R. *Geophysical Research Letters*, *31*(21). https://doi.org/10.1029/2004GL020680

Wang, F., Yang, D., Li, J., Xing, J., & Zhang, G. (2024). Statistical Analysis of Reflected GNSS Signal Off Sea Surfaces From a Coastal Scenario. *IEEE Transactions on Geoscience and Remote Sensing*, *62*, 1–15. https://doi.org/10.1109/TGRS.2024.3500014

Wang, H., Wei, N., Li, M., Han, S. C., Fang, R., & Zhao, Q. (2023). Estimation of GPS-observed ocean tide loading displacements with an improved harmonic analysis in the northwest European

shelf. *Journal of Geodesy*, *97*(12), 0–21. https://doi.org/10.1007/s00190-023-01796-0

Wang, X., Niu, Z., Chen, S., & He, X. (2022). A correction method of height variation error based on one SNR arc applied in GNSS–IR sea-level retrieval. *Remote Sensing*, *14*(1). https://doi.org/10.3390/rs14010011

Wei, Z., Ren, C., Liang, X., Liang, Y., Yin, A., Liang, J., & Yue, W. (2023). Sea-Level Estimation from GNSS-IR under Loose Constraints Based on Local Mean Decomposition. *Sensors*, *23*(14). https://doi.org/10.3390/s23146540

Wei, Z., Ren, C., Liang, Y., Liu, Y., Liang, J., Yin, A., Yue, W., Zhang, X., & Lin, X. (2024). Can the phase of SNR oscillations in GNSS-IR be used to estimate sea-level height? *GPS Solutions*, *28*(3), 1–17. https://doi.org/10.1007/s10291-024-01663-1

Williams, S. D. P., Bell, P. S., McCann, D. L., Cooke, R., & Sams, C. (2020). Demonstrating the Potential of Low-Cost GPS Units for the Remote Measurement of Tides and Water Levels Using Interferometric Reflectometry. *Journal of Atmospheric and Oceanic Technology*, *37*(10), 1925–1935. https://doi.org/10.1175/JTECH-D-20-0063.1

Yalçin, G. (2023). Modeling of Sea Level Changes With GNSS-IR Method and Comparative Analysis With Tide Gauge Data. *Advances in Geomatics*, *1*(1), 32–47. https://doi.org/10.5281/zenodo.10202317

Yang, T., Wang, J., & Sun, Z. (2024). Can the Soil Salinity be Retrieved Using GNSS Interferometric Reflectometry Data? *IEEE Journal of Selected Topics in Applied Earth Observations and Remote Sensing*, *17*, 10612–10620. https://doi.org/10.1109/JSTARS.2024.3391321

Yuan, X., Hu, Y., Liu, W., & Wickert, J. (2024). GNSS-IR Snow Depth Retrieval Based on the PSO-NFP Method With Multi-GNSS Constellations. *IEEE Transactions on Geoscience and Remote Sensing*, *62*, 1–10. https://doi.org/10.1109/TGRS.2024.3492495

Zhu, H., Gui, Y., Shen, Y., Wang, Q., & Zheng, W. (2024). Improving Water Level Retrieval Accuracy of GNSS-IR Based on Ionospheric Refraction Correction Optimization Method. *IEEE Geoscience and Remote Sensing Letters*, *21*, 1–5. https://doi.org/10.1109/LGRS.2024.3451697